Experimental Studies on Belleville Springs use in the Sliding Hinge Joint Connection

Article *in* Journal of Constructional Steel Research · May 2019

DOI: 10.1016/j.jcsr.2019.03.031

5 authors, including:

Shahab Ramhormozian
Auckland University of Technology

George Charles Clifton
University of Auckland

Gregory A. Macrae
University of Canterbury

George P. Davet
Solon Manufacturing Company

Title: Experimental Studies on Belleville Springs use in the Sliding Hinge Joint Connection

Authors: Shahab Ramhormozian[a, *], G. Charles Clifton[b], Gregory A. MacRae[c], George P. Davet[d], Hsen-Han Khoo[e]

[*]Corresponding Author: Shahab Ramhormozian

[a] *Department of Built Environment Engineering, Auckland University of Technology, WZ Building, 6-24 St Paul Street, Auckland, New Zealand*

[b] *Department of Civil and Environmental Engineering, University of Auckland, Engineering Building, 20 Symonds Street, Auckland, New Zealand*

[c] *School of Civil and Natural Resources Engineering, The University of Canterbury, Christchurch, New Zealand*

[d] *Solon Manufacturing Company, Cleveland, Ohio, USA*

[e] *Mitchell Vranjes Consulting Engineers (MV Engineers), 2 Kari St, Grafton, Auckland, New Zealand*

Shahab Ramhormozian: Department of Built Environment Engineering, Auckland University of Technology, WZ Building, 6-24 St Paul Street, Auckland, New Zealand
Email: shahab.ramhormozian@aut.ac.nz

G. Charles Clifton: Department of Civil and Environmental Engineering, University of Auckland, Engineering Building, 20 Symonds Street, Auckland, New Zealand
Email: c.clifton@auckland.ac.nz

Gregory A. MacRae: School of Civil and Environmental Engineering, The University of Canterbury, Christchurch, New Zealand
Email: gregory.macrae@canterbury.ac.nz

George P. Davet: Solon Manufacturing Company, Cleveland, Ohio, USA
Email: gdavet@solonmfg.com

Hsen-Han Khoo: Mitchell Vranjes Consulting Engineers (MV Engineers), Auckland, New Zealand
Email: hsenhan@mvengineers.com

Shahab Ramhormozian: PhD, Lecturer

G. Charles Clifton: PhD, Associate Professor

Gregory A. MacRae: PhD, Associate Professor

George P. Davet: BSME, Chief Engineer

Hsen-Han Khoo: PhD, Senior Structural Engineer

Experimental Studies on Belleville Springs use in the Sliding Hinge Joint Connection

The Sliding hinge joint (SHJ) is a low damage beam-to-column connection developed for and widely used in seismic moment-resisting steel frames (MRSFs). The asymmetric friction connection (AFC) is the SHJ's friction sliding energy dissipating component, which has also been used in other seismic resisting structural systems. In current practice, the AFC bolts are yielded at installation by the method of bolt tightening, and they are subjected to moment, shear, and axial force (MVP) interaction during stable sliding. Hence the AFC bolts tension, and as a result, SHJ elastic strength will be reduced after sliding cycles. A remedy to this post-sliding strength reduction could be installing the AFC bolts in the elastic range in conjunction with using Belleville springs (BeSs) to maintain the clamping force, but at the potential cost of deteriorating the SHJ self-centering capability. This paper describes nine real-scale SHJ's AFC component tests at quasi-static and dynamic rates of displacement controlled loading, with bolts either tightened in the elastic range using no BeSs as well as with four different configurations of BeSs which are deliberately not fully deflected at installation, to avoid the system self-centering capability deterioration and to minimize the additional imposed tension on the AFC bolts during stable sliding. It is concluded that using partially deflected BeSs with sufficient axial deformation to reach the installed bolt tension, with these being installed at both head and nut sides of the AFC bolts, will reduce the post-sliding clamping force loss, improve the self-centering capability, increase the system coefficient of friction, reduce the additional imposed tension on the AFC bolts during stable sliding due to prying actions and/or MVP interactions, and reduce the severity of the sliding surfaces' wearing.

Keywords: Sliding hinge joint, Asymmetric friction connection, Earthquake, Low damage, Belleville spring, Bolt tension loss

1. Introduction

While it is not feasible to design and construct structures to be completely damage resistant under all possible earthquakes, it is readily possible to improve the conventional design and construction approaches to decrease the likelihood and degree of structure damage under severe earthquakes and to significantly raise the structural damage threshold. Low damage design philosophy of structures aims to make the structure occupiable immediately after an ultimate limit state (ULS) event and potentially occupiable in a short time-frame after an event larger than the ULS [1]. Initial key motivation for the low damage design philosophy developments was the experience in the 1994 Northridge [2] and the 1995 Kobe [3] Earthquakes, showing significant unexpected damage to the welded connections of moment-resisting steel frames (MRSFs). While the capacity-designed alternative systems such as reduced beam section (RBS) and bolted flange plate connection [4] could shift such unexpected failures to predictable failures, these systems are yet susceptible to irrecoverable plastic deformations following an event equal to or larger than the ULS event. The low damage design philosophy aims, in addition to satisfying the well accepted “life safety” mandate, to minimize the economic losses due to the post-earthquake damage repair as well as downtime. The importance of this has again been illustrated in further severe earthquakes such as the 2010/2011 Christchurch earthquake series, 2010 Maule earthquake and the 2016 Kaikoura earthquake.

The rotational slotted bolted connection (RSBC) [5] with symmetric friction connections (SFCs) and the sliding hinge joint (SHJ) [6] with asymmetric friction connections (AFCs) are two examples of the low damage beam-column connection developed for seismic MRSFs. The SFC and AFC are two types of the slotted bolted connection (SBC) acting as fuses for the RSBC and SHJ respectively. The SFC and AFC are friction energy dissipating components which are designed to slide at a pre-determined sliding force, under severe earthquake, to dissipate input energy by friction and to limit the maximum beam end bending moment to a pre-determined level, hence effectively preventing any over-loading induced damage to the RSBC and SHJ beam and column. Figures 1 and 2 show the RSBC and SHJ layouts respectively.

The SBCs to be implemented in the seismic resisting systems have been under development for several decades [7-10]. The SBC typically consists of several clamped-by-bolt metal plates in which the interfaces of the plate(s) with slotted holes slide against the interfaces of the plate(s) with normal sized circular holes, when the applied load reaches the frictional resistance of the interface. The influences of the sliding interfaces' material on the seismic behaviour of the SBCs have been researched to improve the SBC's sliding behaviour [11-15]. Both types of the SBC, i.e. SFC and AFC, have been developed into applicable systems, in addition to different configurations of MRSFs. SBC have also been developed for uses other than the MRSFs, such as in steel column bases, steel braces with and without post-tensioning, post-tensioned beam-column connections, eccentrically braced frames (EBFs) with active links, and rocking timber shear walls [11, 16-27].

The SHJ (with AFCs) has been widely used in New Zealand multi-story steel framed buildings. Being subjected to an event larger than the ULS event, the SHJ may undergo large beam-column relative rotation through sliding in two AFCs which are located at the beam web bottom bolt and bottom flange levels, as shown in Figure 2. No lateral movement occurs between the beam and column at top flange level through an axially stiff, rotationally flexible detail. For the events smaller than the ULS, the SHJ is intended to remain rigid. At the end of an earthquake which is larger than the ULS earthquake, the SHJ is ideally intended to come back to its as-built condition. This necessitates the SHJ to dynamically self-center and to retain its as built AFCs' sliding strength through retaining the AFCs' clamping force provided by the initially fully tensioned high strength friction grip (HSFG) bolts. However, it has been shown by researchers that both SFC and AFC may be subjected to the post-sliding bolt tension loss (e.g. [5, 6, 10, 28-32]), with the improvements observed in the experiments using Belleville springs (BeSs), a conical washer type spring. Hence the BeSs have been considered as a potentially beneficial but optional component of the friction sliders, with no experimental research found in the literature focused on investigating their effects and optimum configuration. A downside of retaining the post sliding AFC clamping force could have been deteriorating the self-centring capability of the system through exhibiting resistance to slide while the system tends to come back to its original position. This issue was overcome through the use of partially deflected BeSs as proposed by Ramhormozian et al. [33] and experimentally tested in this research.

This paper describes an experimental research program comprising nine real-scale tests at quasi-static and dynamic rates of displacement controlled loading on the SHJ's beam bottom flange AFC, to investigate the influence of using BeSs on the SHJ's AFC sliding behaviour. The HSFG bolts were installed in the elastic range at ≈50% of the bolt proof load. Different AFC configurations were considered including having no BeSs and having BeSs at one side as well as both sides of the AFC with varying BeS system stiffness values.

This paper provides the answers to the following questions through the results of the experimental research undertaken:

1- What is the SHJ seismic behaviour and what are the reasons for the SHJ's AFC post-sliding clamping loss of bolt force?

2- What is the influence of different configurations of BeSs in the AFC bolt assemblage on maintaining the post-sliding SHJ's AFC clamping force?

3- What is the influence of different configurations of partially deflected BeSs in the AFC bolt assemblage on the self-centering capability of the SHJ's AFC?

4- What is the influence of different configurations of BeSs in the AFC bolt assemblage on the SHJ's AFC system coefficient of friction?

5- What is the influence of different configurations of partially deflected BeSs in the SHJ's AFC bolt assemblage on the clamping force variations during sliding, mainly, due to moment, shear, and axial force (MVP) interaction and/or prying actions?

6- What is the influence of different configurations of BeSs in the AFC bolt assemblage on the AFC sliding surfaces wearing?

2. Sliding hinge joint (SHJ) seismic behaviour

The SHJ (Figure 2) is designed to be rigid under serviceability limit state (SLS) conditions meaning that no sliding in the AFCs is expected, hence the joint acts as a conventional moment resisting frame allowing, ideally, no beam-column relative rotation under the imposed SLS beam end and/or column end bending moment(s) at the joint. Under the event greater than the ultimate limit state (ULS) events, the SHJ is expected to become semi rigid, meaning that sliding in the AFCs is expected. This allows beam-column relative rotation to occur about the point of rotation to dissipate energy through AFCs friction sliding, and to limit the beam end bending moment to a pre-determined level to prevent the beams and columns to exhibit inelastic behaviour. This pre-determined bending moment level is directly related to the frictional resistance of the AFCs. The SHJ's point of rotation is located at the top flange plate to isolate the floor slab. Moreover, the SHJ decouples the joint's elastic strength and elastic rotational stiffness providing a high versatility to optimize the beam size under ULS events and still satisfying the SLS deflection limits. The SHJ is ideally expected to seize up and become rigid again at the end of a severe earthquake beyond the ULS event.

The SHJ moment-rotational behaviour is dependent on and similar to the AFC force displacement behaviour. Figure 3(a) shows the AFC configuration at the SHJ beam bottom flange. The AFC consists of five plies, including the beam bottom flange, bottom flange plate (cleat), cap plate, and two shims at both sides of the cleat, all clamped by the pre tensioned high strength friction grip (HSFG) structural bolts. All of the AFC plies have normal size holes except the cleat having slotted holes to allow sliding. In current practice, the AFC plies are all made of mild steel, except the shims which are made from high hardness (abrasion resistant) steel [15], and the AFC HSFG bolts are fully tensioned at installation (i.e. yielded) with the turn-of-nut method in accordance to the New Zealand Steel Structures Standard, NZS 3404 [34].

The AFC has two main sliding surfaces at both sides of the cleat. The force displacement behaviour of the AFC is shown in Figures 3(b) and 11. With reference to Figure 3(b), when the applied force overcomes the frictional resistance of the first sliding surface, i.e. the cleat and the upper shim interface, this surface starts to slide (i.e. cleat moves relative to the beam bottom flange), while the cap plate remains fixed relative to the cleat and moves relative to the beam bottom flange (shown as B). After a short time or distance of movement along the first sliding surface, the cap plate starts to become fixed in position relative to the beam bottom flange. From this point onwards for that direction of displacement, the cleat slides between two sliding surfaces (i.e. upper and lower shims), which almost doubles the sliding shear resistance (called the stable sliding shear resistance) developed by the AFC (shown as C). At this stage, the bolts are pushed into the double curvature state. Following load removal and then load reversal, the sliding occurs on the first interface (shown as D) followed by the second interface (shown as E) pushing the bolts again into double curvature in the opposite direction. This provides the AFC with a “pinched” hysteretic behaviour, requiring less work to be done (or energy to be spent) to recover all of the travelled displacement compared with a SFC’s rectangular typical hysteretic behaviour.

The AFC is subject to a post-sliding clamping force reduction because of the following reasons:

1. The MVP interaction in the bolt body during stable sliding state [12, 35] may yield the bolt material causing the post-sliding bolt tension to drop. It is worth noting that the bolts are currently tensioned into the post yield condition at installation in practice making this reduction inevitable.
2. The prying effect at the SHJ beam bottom flange level under large beam-column relative rotation may impose an additional axial plastic strain on the AFC bolts causing the post-sliding bolt tension to reduce.
3. Wearing of the sliding surfaces may reduce the total thickness of the AFC plies per bolt, resulting in the bolt tension reduction.
4. AFC bolts may rub against sides of the cleat elongated holes. This may reduce the AFC bolts' integrity, causing a bolt tension drop.
5. Vibration induced self-loosening, joint creep, and bolt relaxation are amongst the common bolt tension loss reasons that may be considered for any bolted connection amongst which the AFC may not be an exception.

3. SHJ's beam bottom flange AFC real-scale component tests description

3.1. Test rig and AFC plies

A test rig (Figure 4) was designed and used to simulate the sliding behaviour of the SHJ beam bottom flange AFC assemblage. It consists of a column hinged to a strong wall base plate at A, through a very low friction bearing, connected to a ±300 kN Shore Western (SW) dynamic actuator at B, and having four threaded holes and a circular shear key to bolt and hold the cleat at C. A beam flange plate was bolted to the strong wall base plate to allow assembling the AFC component for each test. This test setup is an inverted representation of the SHJ, with the point of rotation at A, and the SHJ beam bottom flange AFC at C. The SW dynamic actuator applies the quasi-static as well as intermediate and main dynamic displacement controlled loads at B. The loading regime is explained in Section 3.5 below.

The vertical distance between the hinge centre and the cleat top surface, where the AFC plies relative displacements are measured, is 478 mm, a figure which closely represents a beam section depth of a 460 UB section. The reaction arm amplifies the load from that applied by the SW dynamic actuator at B by a factor of 2.24, if the system is assumed as static with a perfectly friction-less bearing at A, generating the required AFC sliding force transferred to the cleat through the shear key at C. Assuming the system as dynamic, the test rig column can be considered as a generalized single degree of freedom (SDOF) dynamic system [36]. However, since the imposed loads are orders of magnitude higher than the mass generated inertia forces, as a result of the absence of the dead (permanent) and live (imposed) contributing building mass, it is acceptable here to use the factor of the static system also for the dynamic system. The distance from the hinge centre and the centre of the actuator connection plate to the column is 1071mm. Hence, the load amplifying factor, or the displacement decreasing factor assuming a rigid body rotation (RBR) for the column, is (1071/478)=2.24.

Each test specimen comprised a beam flange plate, a cleat, and a cap plate on top, all of which are schematically shown in Figure 4. The beam flange plate was 16 mm thick with 22 mm diameter plasma cut circular holes and was bolted to the strong wall base plate. The narrow end of the cleat was 243 mm × 150 mm × 16 mm with 57 mm long elongated plasma cut holes, with the wider end bolted to the top of the column and held by the circular shear key. The cap plate was 175 mm × 150 mm × 16 mm with 22 mm diameter plasma cut circular holes. These plates were made from Grade 350 steel (typical f_y=350-440MPa and typical hardness=147-189HV). The 5mm thick high hardness (wear or abrasion resistant) steel shims were made from Raex 450 grade plate (typical f_y=1200MPa and hardness range=442-526HV). The shims were 190 mm × 175 mm including 22 mm diameter plasma cut circular holes and were placed at both sides of the cleat. The plies surfaces were sweep blasted to St2 surface finish standard [37]. A new cleat was used for each experiment. The shims used for each experiment were either new or reused from the previous experiments, with the unscratched main sliding surface facing the cleat in the new experiment. Hence the shims were effectively new for each test.

3.2. Bolts and Belleville springs

The M20 galvanized HSFG property class (PC) 8.8 steel structural bolts were supplied by a specialist New Zealand fasteners supplier to AS/NZS 1252 [38] and used for the experiments. New bolts were used for each experiment. Table 1 shows the nominal characteristics of the bolts.

The BeSs were supplied by a specialist American Belleville Spring manufacturing company. Table 2 shows the characteristics of the BeS “M20-52-6.0NF/S1” tested before being used in the experiments. The BeSs were all pre-set by the manufacturer, meaning that they were loaded to a flat disc once after the production, hence behaved fully elastically in the experiments. Pre-setting is essential for BeS’s used in this system. Consequently, the BeSs were re used for different experiments. The load-deflection values of the M20-52-6.0NF/S1 BeS are shown in Table 3 and the associated loading as well as unloading curves are demonstrated in Figure 5 along with a fitted linear line originated at (0,0) to represent both loading and unloading data points the best indicating the nominal stiffness of 135kN/mm for each BeS. A detailed discussion on the BeS’ characteristics may be found in [33].

3.3. AFC Bolts and Belleville springs assemblage configurations

50% of the HSFG property class 8.8 M20 bolt proof load i.e. 0.5×147=73.5kN was considered as the target installed bolt tension for all of the experiments. This is to keep the bolts in the elastic range at installation, increasing their capacity to accommodate additional elastic stresses during stable sliding. Five different configurations were considered for the use of BeSs namely: 1) NS-Ti, 2) S1-Ti, 3) S2-Ti, 4) S3-Ti, and 5) S4-Ti. These designations mean; 1) having no BeSs but ordinary HSFG hardened washers, and 2) to 5) having one, two, three, and four BeSs in series respectively. A detailed discussion on the BeS' possible series, parallel, and series/parallel assemblage configurations may be found in [33]. Ti=1, 2, and 3 represent the number of each specific configuration's test repeat. The configurations S2 and S4 used one Belleville spring at nut side between a hardened washer under the nut and the cap plate while the configurations NS, S1, and S3 used only the HSFG hardened washer under the nut. Configurations S1 and S2, and S3 and S4 used 1 and 3 BeSs at head side of each bolt respectively. Considering the joint grip length, the values for the bolt lengths that were used for the experiments were 110mm, 120mm, 120mm, 130mm, and 140mm for NS-Ti, S1-Ti, S2-Ti, S3-Ti, and S4-Ti respectively, all excluding the bolt head thickness. This ensured that the full height of the nut was engaged with the bolt threaded part by showing at least one clear thread above the nut after tightening, as is recommended by [34]. Figure 6 shows different configurations of the bolts and BeSs assemblage.

3.4. SHJ's AFCs assemblage and test measurements

The AFC bolts were tightened in sequence from the first one to the forth one, first, up to snug tight according to [34], then from the first one to the fourth one up to the desired level of tension using a V-RAD-16 electric torque multiplier. The bolts were numbered as is shown in Figure 6f. It is worth noting that a better sequence for tightening a bolted connection with each bolt having the same boundary condition stiffness would be 1, 3, 4, 2, however according to NZS3404 [34] recommendations for assembly of a connection involving tensioned bolts, snug-tightening and final tensioning of the bolts in a connection shall proceed from the stiffest part of the connection towards the free edges and that was done in this instance. The four bolts' tension was monitored and recorded continuously over the whole test time by four Transducer Techniques TT-LWO-60 load cells (Figure 6). Each load cell was sandwiched between two M20 HSFG hardened washers, and each load cell's capacity was 267kN.

The relative displacements between the AFC plies were recorded by five portal displacement gauges (Figure 6). The displacement and axial force of the actuator were recorded by the actuator internal displacement gauge and load cell. The actuator was connected to the test rig column by four pre-tensioned structural bolts. The bracket supporting the actuator load and the strong wall base plate were installed on the strong floor and strong wall respectively, each one by seven post tensioned rods to minimize support movement. A number of trials were performed at first to determine the calibration factor of the test rig due to the sources of potential flexibility and slip. The aim was to evaluate the maximum necessary displacement of the actuator resulting in the maximum desired displacement of the AFC cleat. These trials were performed using the AFC bolts tightened up to 50% of the proof load as was the case for the main tests. The calibration factor was determined as 1.5. After these trials, the bolts of the test rig connections, especially the actuator connections, were firmly retightened to minimize the system slip during the main tests.

The length of each bolt was measured by an ultrasonic G5 bolt tension meter, before tightening, after tightening, after each test, and after untightening (Figure 6). The bolt head and the nut were marked so as to investigate if there has been any nut relative to bolt head rotation during the sliding tests. The temperatures of the bolts were measured before the test, right after the main dynamic loading, and after the test using a laser point infrared digital thermometer gun (Figure 6h). The height of the BeSs "at both sides if applicable" was measured by a depth micrometre before and after the test (Figure 6e).

3.5. Loading regime

The loading regime comprised a combination of displacement controlled load histories, namely a main dynamic loading pattern, four quasi-static, and four intermediate dynamic regimes. The loading regime was designed to simulate the pre-earthquake, severe earthquake, and post-earthquake conditions to represent a combination of SLS, ULS, and greater than ULS events. The loading regime displacement versus time is shown in Figure 7.

The Quasi-static loading provides an AFC cleat-beam flange plate relative displacement of approximately 4.8 mm, corresponding to a SHJ beam-column relative rotation of 0.010 rad which was applied at a slow slip rate of 1 mm/minute. The displacement controlled Quasi-static load was in both positive and negative directions as is shown in Figure 7.

Following each Quasi-static loading, the intermediate dynamic load was applied to ensure that the AFC cleat-beam flange plate relative displacement was gradually reduced and the AFC bolts ended up close to straight state, i.e. not the double curvature state. The number of cycles consisted of five cycles each to 3.6 mm and 2.4 mm, followed by nine cycles of decreasing amplitudes, as is shown in Figure 7.

The main dynamic load was applied after an intermediate dynamic loading, in the middle of the whole loading, as is shown in Figure 7, consisting of 3 AFC cleat-beam flange plate relative displacement cycles to 2.4 mm and 3.6 mm, 2 cycles to 4.8 mm, 1 cycle to 7.2 mm and 9.6 mm, 2 cycles to 14.3 mm, and back down again. This corresponds to SHJ beam-column relative rotations of 0.005 rad, 0.0075 rad, 0.010 rad, 0.015 rad, 0.020 rad and 0.030

rad. It is worth noting that the higher amplitudes mentioned above push the SHJ's AFC beyond the limits associated with the 2.5% ULS inter-storey drift which is specified by [39].

For the amplitudes less than or equal to 3.6mm, the period of the loading was T=1sec/cycle, and for the amplitudes greater than 3.6mm, the period was T=1.5sec/cycle. This is because, the higher the SHJ's AFC sliding displacements, or the damage in a non-low damage MRSF building, are associated with the higher periods. The loading regime was modified in this research, to represent pre-earthquake, severe earthquake, and post-earthquake conditions, from that initially adapted by [6, 28] from the recommended testing procedure for MRSFs by [40].

4. Results and discussions

Five tests were first carried out for each configuration followed by two more repeats on each one of the NS and S4 configurations that showed the less-than and the most desirable seismic behaviour respectively, particularly in terms of post sliding clamping force retention. Hence a total of nine tests were carried out. The details of the test specimens are shown in Table 4. The values on the table are calculated as follows in which D is calculated based on linear interpolation using load-deflection data points presented in Table 4, E is the BeS system nominal reserved deflection up to a flat BeS system considering 0.84mm as the flat deflection of each BeS, and j is the number of BeSs in each test bolt assemblage configuration:

$$A = AFC\ installed\ clamping\ force = \sum_{k=1}^{4} k^{th}\ AFC\ bolt\ installed\ tension$$

$$B = Average\ AFC\ installed\ bolt\ tension = \frac{A}{4} \times \left(\frac{100}{bolt\ proof\ load = 147kN}\right)[\text{Actual (\%)}]$$

$$C = Nominal\ stiffness\ of\ the\ BeS\ system = \frac{Nominal\ stiffness\ of\ one\ BeS = 135kN/mm}{Number\ of\ Belleville\ springs\ in\ series = j}$$

$$D = Average\ nominal\ deflection\ of\ the\ BeS\ system\ at\ installation = j \times \left\{\left[(B - 55.7) \times \frac{0.63 - 0.43}{85.4 - 55.7}\right] + 0.43\right\}$$

$$E = Average\ nominal\ reserved\ deflection\ of\ the\ BeS\ system\ at\ installation = (0.84 \times j) - D$$

4.1. SHJ's AFC elastic strength reduction

Table 5 shows the percentage of post-sliding AFC clamping force loss at the end of each test with respect to the installed clamping force as well as the AFC post sliding force threshold of losing stiffness normalized to the installed clamping force, for different configurations. These are named the normalized clamping force loss (CFL) and the normalized elastic strength limit (ESL) respectively. The force threshold of stiffness loss is defined as the point on the last quasi static loading line at which there is a significant reduction in the system stiffness or strength, suggesting the sliding has occurred.

The S1 and S2 configurations have not made an improvement on the CFL value compared with the cases without BeSs. The first reason is that the average nominal total deflection of the BeSs at installation for these two configurations are not sufficient to efficiently retain the bolt tension. The second reason is that the accurate readings of the load cells were gained at the loads higher than 20-30kN. The loads lower than this level might have been considerably smaller than the recorded values. Hence, it is possible most likely that the AFC of the NS, and less likely S1 and/or S2 cases had lost their clamping force even more than what is shown in Table 5. The third reason is that the bolt tension readings of the S1 and S2 configurations were generally electrically noisy, and unrealistically low during stable sliding state, resulting in an unrealistically high calculated stable sliding system coefficient of friction. This could have been the case with the readings at the end of these tests too. The post sliding elastic strength reduction factor (SRF) is defined as the ratio of CFL and ESL ($SRF = \frac{CFL}{ESL}$) shown in Table 5. The smaller SRF means more retention of the post sliding elastic strength. Figure 8 shows the improved retention of the AFC elastic strength through the use of BeSs. The S1 and S2 results are shown in red in Table 5 and are not shown in Figure 8 because of the reasons given above. The coefficient of variation (CV) of the post sliding elastic strength limit for S4 tests is CV=0.08, showing more stable behaviour compared with NS configurations with CV=0.19. Although the coefficient of variation of clamping force loss for the NS tests is recorded as less than that of the S4 tests, this is mainly because of the load cell's low accuracy in capturing low values of the bolt tensions, as is explained above, hence is not reliable.

The average nominal total deflection of the BeSs at installation was 0.52mm and 1.09mm respectively for S1 and S2. An average of 62% of the AFC clamping force was lost for the NS, S1, and S2 tests (59% for the NS tests). It is worth noting that the bolts are currently fully tensioned at installation in practice suggesting more expected bolt tension loss compared with NS tests using the bolts installed in the elastic range. The average nominal total deflection of the BeSs at installation for the S3 and S4s configurations were 1.62 and 2.25mm respectively. This was sufficient to compensate for most of the bolt tension loss, meaning that an average of 37% of the installed clamping force was lost for the S3 and S4 tests (37% also only for S4 tests) following the whole sliding regime. It is worth noting that using one equivalent BeS instead of two or more BeSs in series (at each side of the bolt), such as S3 and S4, is more efficient in delivering the nominal BeSs deflection as shown experimentally by Ramhormozian et al. [41]. This is principally because the BeSs in series configuration may experience stack slippage in service resulting in deterioration in their functionality and efficiency, as this slippage was observed in the experiments. An equivalent BeS instead of two or more BeSs in series is also more cost effective [33] and simpler to be used in practice.

To have a suitable BeS system being able to compensate for most of the AFC post sliding clamping force and elastic strength loss, it is necessary that the BeS system deflects as much as possible at the time of installation up to the installed bolt tension. In other words, the stiffness of the BeS system should be smaller than that of the bolt and plies as much as possible, and still having a flat load not less than the installed bolt tension. This action is analytically formulated by Ramhormozian et al. [33].

4.2. SHJ’s AFC total bolt tension increase due to prying and/or MVP interaction, and the stable sliding force

Table 6 shows the percentage of the AFC stable sliding (SS) maximum total bolt tension increase with respect to the AFC resting total bolt tension (when the bolts are ideally straight) just before the main dynamic loading regime. The average percentage of the AFC stable sliding (SS) maximum total bolt tension increase was 53% for the NS tests and 14.3% for the S3, and S4 tests (13.7% for the S4 tests). This shows significant less additional imposed tension to the SHJ’s AFC bolts during stable sliding, resulted from MVP interaction and/or prying actions, attributed to the partially (not fully) deflected BeSs. Although the coefficient of variation of stable sliding (SS) maximum total bolt tension increase for NS tests is less than that of S4 tests, this may be because of the load cell’s low accuracy in capturing low values of the bolt tension. (The low values of the bolts tension in resting state might have been considerably smaller and more variable than the recorded values, suggesting even higher SS maximum total bolt tension increase for the NS tests, as is mentioned in section 4.1).

Table 6 also shows the average AFC SS force normalized to the installed clamping force. This is presented as the mean value of all data points over the stable sliding hysteresis loop in SS +ve and –ve directions, and then an average of the mean values of +ve and –ve SS forces. This is a fair representation of the SHJ SS behaviour, as in a real building, the SHJs of an internal MRF column slide simultaneously in +ve and –ve directions during a severe earthquake. The two external columns’ SHJs of a MRF similarly slide simultaneously in +ve and –ve directions. The average SS force normalized to the installed clamping force was 1.04 for the NS tests and 1.11 for the S1, S2, S3, and S4 tests (1.14 for the S4 tests), meaning that, although using partially deflected BeSs significantly decreases the additional imposed tension on the bolts (or clamping force) during SS, they can yet deliver slightly higher SS force with respect to the installed clamping force. This is due to factors such as 1) retention of the clamping force and 2) providing higher system coefficient of friction (when used at both sides of the bolt), as explained in section 4.3 below. The coefficient of variation for the average SS normalized force is less than 0.1 for both NS and S4 tests. Figure 9 shows the percentage of the AFC SS maximum total bolt tension increase with respect to the AFC resting total bolt tension (when the bolts are ideally straight) just before the main dynamic loading regime (excluding S1 and S2 tests as is explained before) as well as the average AFC SS force normalized to the installed clamping force for all tests.

To have a suitable BeS system being able to minimize the additional SS imposed bolt tension due to MVP interaction and/or prying actions, it is necessary that the BeS system is partially (not fully) deflected providing a degree of longitudinal flexibility under the bolt head and/or nut compared with the conventional layout or the case with fully deflected Belleville springs. A design procedure for the use of BeSs in the SHJ to achieve this goal is proposed in [33].

4.3. SHJ's AFC stable sliding system coefficient of friction

Table 7 shows the average AFC SS system coefficient of friction (CoF). This is presented as the mean value of all data points over the stable sliding hysteresis loop in SS +ve and –ve directions, and then an average of the mean values of +ve and –ve SS forces. As is already mentioned in section 4.2, this is a fair representation of the SHJ SS behaviour in a real building. The CoF is calculated over the time using the following equation.

$$SS\ CoF = \frac{Actuator\ imposed\ load \times 2.24}{2 \times \sum_{K=1}^{4} K^{th}\ AFC\ bolt\ tension}$$

The average SS system CoF was 0.58 for the NS tests, 0.59 for the S3 test, and 0.72 for the S4 tests showing that, the use of BeSs at both head and nut sides (not only one side) of the AFC bolts with the BeS wider edge facing the underneath plates can increase the system coefficient of friction. This is attributed to the wider contact area along the AFC sliding interfaces, being clamped under a wider area at both outer sides of the AFC [33, 42]. The coefficient of variation for the average SS system CoF is 0.08 and 0.03 for NS and S4 tests respectively, showing more stable average SS system CoF for the case with BeSs. Figure 10 shows the average SS system CoF for all tests excluding S1 and S2 as is explained in section 4.1.

To have a suitable BeS system being able to maximize the AFC SS system CoF, it is recommended that the BeSs are used at both head and nut sides of the bolts with the wider edge facing the underneath plate. This also has advantages if the joint is to be painted post BeS application as it will prevent paint from getting under the BeS surface and impeding the ability of the BeSs to compress fully during sliding.

4.4. SHJ's AFC self-centering capability

Three parameters are defined to investigate the self-centering capability of the SHJ's AFC, namely: re-centering energy ratio (RCER), normalized re-centering force (RCF), and normalized re-centering distance (RCD). The RCER is defined as the ratio of the amount of energy dissipated in both +ve and –ve directions under loading, to the amount of energy required to be spent to bring the system back to its zero-displacement state. This ratio is 1 for a perfectly rectangular hysteresis loop and 0 for a perfectly self-centering (flag-shaped) hysteresis loop. To calculate the RCER, all of the large amplitude SS hysteresis loops of the experiments were stretched or shortened in +ve and –ve displacement directions (along x axis) from zero displacement points with respect to the force (y) axis, to ensure that the absolute value of the maximum reached displacement is exactly 14.3mm for all of the considered hysteresis loops. The RCER then is calculated using the following equation.

$$RCER = \frac{\left|\int_{1^{st}\ and\ 3^{rd} quadrants} F(x)dx\right|}{\left|\int_{2^{nd} and\ 4^{th} quadrants} F(x)dx\right|} \cong \frac{\sum_{i=1}^{n-1}\left|\frac{F_i + F_{i+1}}{2} \times (x_{i+1} - x_i)\right|}{\sum_{i=1}^{m-1}\left|\frac{F_i + F_{i+1}}{2} \times (x_{i+1} - x_i)\right|} = \frac{E_1 + E_3}{E_2 + E_4}$$

where F=imposed load on the AFC cleat, x=relative displacement between beam flange plate and cleat, n=number of data points on the 1^{st} and 3^{rd} quadrants of the AFC hysteresis loop, m= number of data points on the 2^{nd} and 4^{th} quadrants of the AFC hysteresis loop, and E_i=area under the force-displacement graph in the i^{th} quadrant.

The normalized re-centering force (RCF) is defined as the force, normalized to the associated average stable sliding force (either +ve or –ve), at which the connection significantly loses its stiffness, suggesting the initiation of sliding in the first sliding interface while the imposed force tries to bring the connection back to its initial position in 1^{st} and 3^{rd} quadrants of the AFC hysteresis loop. The normalized re-centering distance (RCD) is defined as the total travel of the cleat relative to the beam flange plate from the maximum reached +ve and –ve relative displacement in 2^{nd} and 4^{th} quadrants of the AFC hysteresis loop, to the point at which the full AFC frictional resistance, resulted from two active sliding interfaces (i.e. SS state), starts to be developed in the in 1^{st} and 3^{rd} quadrants of the AFC hysteresis loop. This is normalized to the maximum nominal displacement i.e. 14.3mm. Figure 11 schematically shows E_i, RCF, and RCD on an AFC hysteresis loop. The self-centering factor (SCF) is defined as ($SCF = \frac{RCER \times RCF_{average}}{RCD_{average}}$). The smaller SCF suggests more AFC tendency for self-centering. Table 8 shows the values of RCER, RCF, RCD, and SCF for all nine experiments.

Figure 12 shows that the use of Belleville springs, which are partially deflected, does not deteriorate but has a beneficial influence on the AFC self-centering capability, meaning that the values of RCER and RCF are decreased and the value of RCD is increased in presence of partially deflected BeSs. This causes the SCF to be considerably decreased in presence of partially deflected BeSs. This is attributed to the rotational flexibility under the bolt head and/or nut provided by not flattened BeSs during stable sliding state, allowing the bolt body to rotate and provide a tendency for self-centering [33]. This improvement is maximum for the S2 configuration with SCF of 0.06 compared with average SCF of 0.58 for NS configurations, given existence of this rotational flexibility at both head and nut sides with one BeS at each side. S3 and S4 configurations used three BeSs in series at head side of the bolt. This makes a constraint around the shank at head side to rotate efficiently during stable sliding, hence S3 and S4 configurations (with SCF and average SCF of 0.23 and 0.27 respectively) are not as efficient as S2 configuration from the self-centering point of view, although their axial flexibility is higher than that of S2 configuration. The SCF value for S1 configuration was 0.27. In summary the self-centering capability of the system was considerably improved for all test specimens that used the partially deflected BeS system.

To have a suitable BeS system being able to maximize the self-centering capability of the AFC, it is necessary that two BeSs, one under the head and one under the nut, are used being partially (not fully) deflected to provide a degree of rotational flexibility under the bolt head and nut at the same time during stable sliding generating the horizontal self-centering tension components of the rotated bolt. Table 8 shows that the average nominal reserved deflection of the BeS system for S2 configuration, which showed the most satisfactory self-centering capability, was 0.58mm (0.29mm for each BeS) at installation. A design procedure for the use of BeSs in the SHJ to achieve this effect is proposed in [33].

4.5. Other observations

The use of BeSs could generally decrease the extent and severity of the friction sliding resulted wearing of the sliding surfaces known also as galling, as can be seen in Figure 13, showing the abrasion resistant shims' interface with the cleat at the beam bottom flange side, for a NS and the S2 configuration. This is through the wider distributed clamping force along the edges of the BeSs compared with more localized clamping force transferred through the hardened washers. It is recommended to use the BeSs with the highest practical outside diameter used at both sides of the AFC to maximize this desirable effect.

The temperature rise during sliding was found to be an un-important parameter, with a bolt temperature rise of not more than 4 degrees Centigrade; not sufficient to influence the AFC bolt behaviour. Using depth micrometre to measure the BeSs height change before and after the tests was found to be not an accurate method, although the measurements generally showed that the BeSs pushed out following each test to help in avoiding the bolt tension drop. The ultrasonic G5 tension meter measurements were slightly and unrealistically larger than theory based expectations suggesting a need for a device overhaul. However the recordings showed that all of the bolts were longer after removing at the end of each test compared with the initial length. This suggests a degree of potential plastic elongation even with the AFC bolts installed in the elastic range. Moreover no turn of the nut was observed during the tests.

5. Conclusions:

1- The SHJ is a low damage beam-column connection developed for and used practically in the seismic resisting MRSFs. The SHJ uses the AFCs as the friction energy dissipaters to dissipate energy through sliding under an event greater than the ULS event. The AFC has been researched to be used in other types of seismic resisting systems than only the MRFs. The SHJ develops a non-linear inelastic moment-rotation hysteresis curve. The conventionally fully tensioned SHJ’s AFC bolts are highly susceptible to the post stable sliding tension loss because of the MVP interaction, prying actions, wearing of the AFC plies sliding surfaces and reduction in the plies thickness per bolt. These are a combination of potential initial, short term, and long term bolt tension loss factors.

2- A BeS system which can develop reasonably large deflection at the time of installation up to the installed bolt tension (≈2mm), i.e. with the stiffness reasonably smaller than that of the bolt/joint and yet with a flat load not less than the installed bolt tension, would be able to compensate for most of the AFC post sliding clamping force and elastic strength loss. The average percentage of the AFC clamping force loss with respect to the initial clamping force of the NS configurations was at least ≈60% higher than that of the S4 configurations.

3- Using two BeSs, one under the AFC bolt head and one under the nut, which are partially (not fully) deflected at installation (≈0.6mm of reserved deflection for the BeS system), will provide a degree of rotational flexibility under the bolt head and nut during stable sliding generating the horizontal self-centering tension components of the rotated bolt. This will significantly enhance the SHJ self-centering capability.

4- Using BeSs at both head and nut sides of the AFC bolts with the wider edge facing the underneath plate increases the AFC stable sliding system coefficient of friction (by ≈25%). To maximize this effect it is recommended to use the BeSs with maximum possible outside diameter. This makes it also easier for the manufacturer to customize the designed BeSs with the desirable flat load and deflection. moreover, this has the added benefits of increasing deflection and greater consistency in BeSs load versus deflection performance

5- The partially (not fully) deflected BeS system at installation provides a degree of longitudinal flexibility under the AFC bolt head and/or nut minimizing the additional stable sliding (SS) imposed bolt tension with respect to the bolt tension in straight state, due to the MVP interaction and/or prying actions. This is in comparison with the conventional layout or the case with fully deflected BeSs. This bolt tension increase was at least ≈290% greater for the NS configuration compared with the S4 configuration. This effect does not reduce the AFC stable sliding force with respect to its initial total clamping force, as the average stable sliding force normalized to the installed clamping force was even ≈10% higher for the S4 configuration compared with the NS configurations as a result of the factors such as retention of the clamping force and providing higher system coefficient of friction.

6- The use of BeSs will generally decrease the extent and severity of the friction sliding resulted wearing of the sliding surfaces through the wider distributed clamping force along the edges of the BeSs compared with more localized clamping force transferred through the hardened washers. Hence it is recommended to use the BeSs with the highest practical outside diameter used at both sides of the AFC to maximize this effect.

6. Acknowledgements

The experiments of this research were financially supported by Earthquake Commission Research Foundation (Project 14/U687 “Sliding Hinge Joint Connection with BeSs”). The authors are grateful for this support. The first author PhD studies at the UoA was financially supported through a QuakeCoRE PhD scholarship. This support is much appreciated. The efforts and help of the technical and laboratory staff at the Department of Civil and Environmental Engineering, the UoA as well as final year BSc Eng. students, Raghav

Kruthiventy and Jay Dangwal, helping in conducting experimental testing is also acknowledged. The Authors would also like to extend special thanks to D&H Steel, Steelmasters, EDL, Solon Manufacturing, and TT load cell companies for helping in supplying the experiments components.

Table captions

Table 1. Nominal characteristics of the galvanized HSFG PC 8.8 structural steel bolts

Table 2. Characteristics of each BeS “M20-52-6.0NF/S1”

Table 3. Load-deflection values of the BeS “M20-52-6.0NF/S1”

Table 4. Details of the test specimens

Table 5. Percentage of post-sliding AFC clamping force loss, normalized force threshold of losing stiffness, and elastic strength reduction factor.

Table 6. Percentage of SHJ’s AFC stable sliding maximum total bolt tension increase and average stable sliding normalized force.

Table 7. SHJ’s AFC average stable sliding coefficient of friction.

Table 8. SHJ’s AFC re-centering energy ratio, normalized re-centering force, normalized recentering distance, and self-centering factor

Figure captions

Figure 1) The rotational slotted bolted connection (RSBC) layout [5]

Figure 2. The sliding hinge joint (SHJ) views (a) front (b) beam cross sectional, (c) back, and (d) 3D [33]

Figure 3. (a) AFC in the beam bottom flange and (b) AFC idealized force-displacement behaviour [43]

Figure 4. SHJ’s AFC test setup (a), schematic of the SHJ’s AFC test specimens (b), SW 300kN dynamic actuator (c), and SHJ’s AFC test rig (d)

Figure 5. Loading and unloading curves of the BeS along with the fitted stiffness line

Figure 6. SHJ’s AFC assembled component with portal gauges installed (NS or S1 or S3 configurations) (a), SHJ’s AFC bolts at head side with donut load cells (NS configuration)

(b), and (S3 or S4 configurations) (c), using depth micrometer to measure BeSs deflections at SHJ's AFC bolts' head side (S1 or S2 configurations) (d), using depth micrometer to measure BeSs deflections at SHJ's AFC bolts' nut side (S2 or S4 configurations) (e), SHJ's AFC bolts numbering (NS or S1 or S3 configurations) (f), and using G5 ultrasound bolt tension meter to measure SHJ's AFC bolts lengths (g).

Figure 7. The loading regime consisting of quasi-static, intermediate dynamic, and main dynamic displacement controlled load histories.

Figure 8. SHJ's AFC normalized clamping force loss (a) and elastic strength limit (b), and elastic strength reduction factor (c)

Figure 9. SHJ's AFC stable sliding maximum total bolt tension increase (a) and average stable sliding normalized force (b)

Figure 10. SHJ's AFC average stable sliding coefficient of friction.

Figure 11. SHJ's AFC schematic stable slding hystheresis loop showing stable sliding force, re-centering force, recentring distance, and dissipated energy in each quadrant.

Figure 12. SHJ's AFC re-centering energy ratio (a), normalized average re-centering force (b), normalized average recentering distance (c), and self-centering factor (d).

Figure 13. extent of the slding resulted scratches on the abrasion resistant shim facing the cleat at the SHJ beam bottom flange side for the NS configuaration (left) and S2 configuration (right).

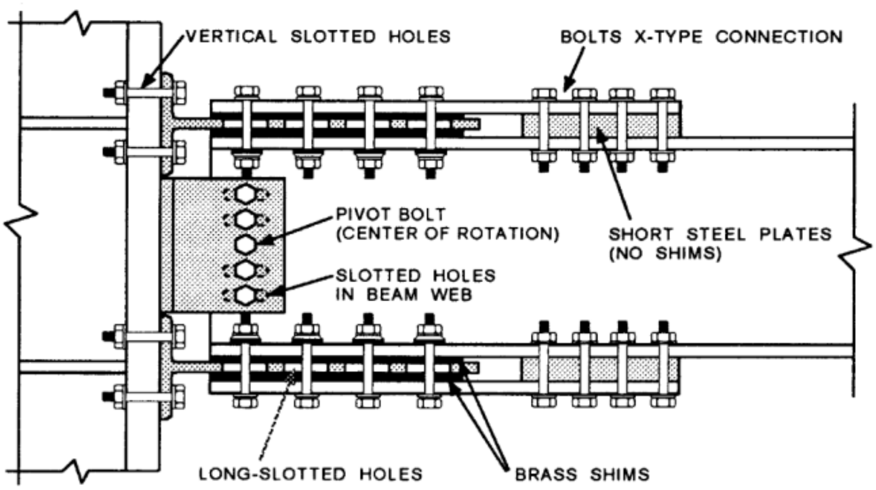

Figure 1) The rotational slotted bolted connection (RSBC) layout [5]

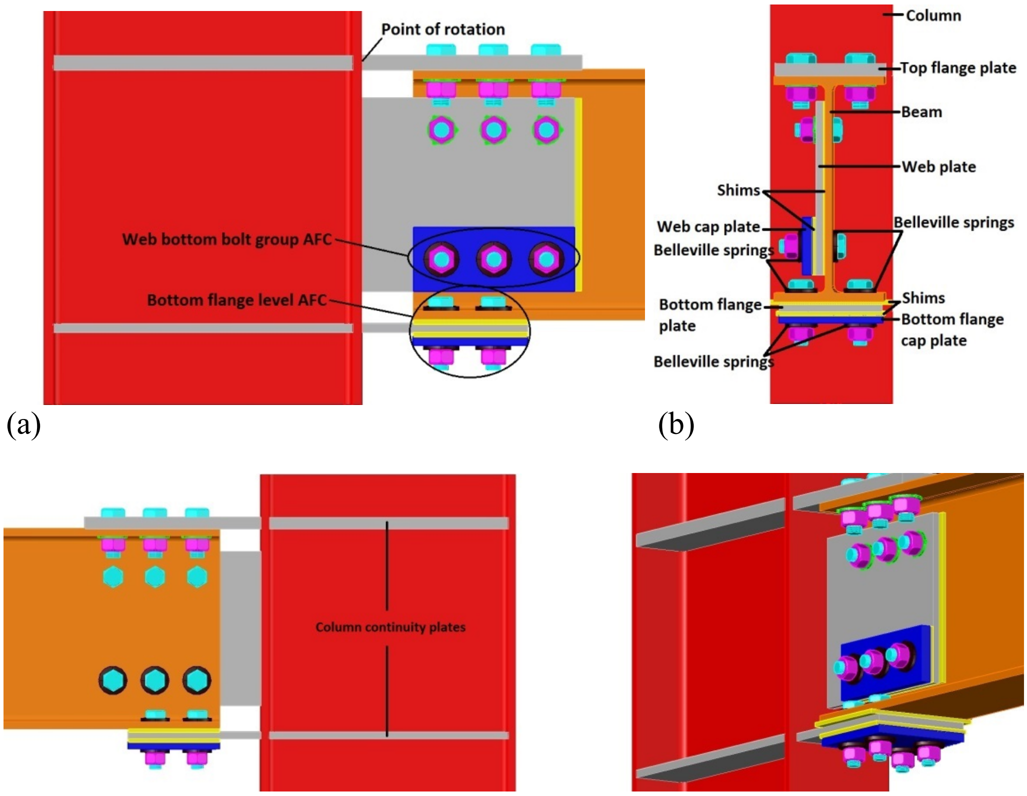

(a) (b)

(c) (d)

Figure 2. The sliding hinge joint (SHJ) views (a) front (b) beam cross sectional, (c) back, and (d) 3D [33]

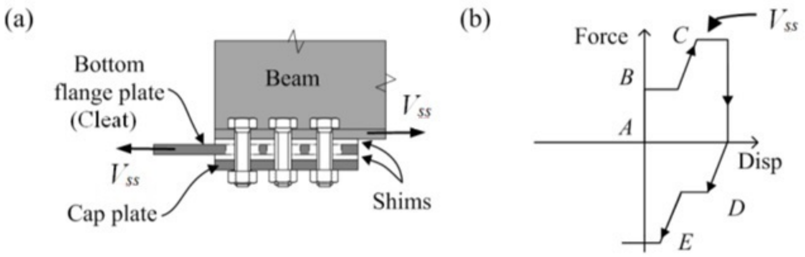

Figure 3. (a) AFC in the beam bottom flange and (b) AFC idealized force-displacement behaviour [43]

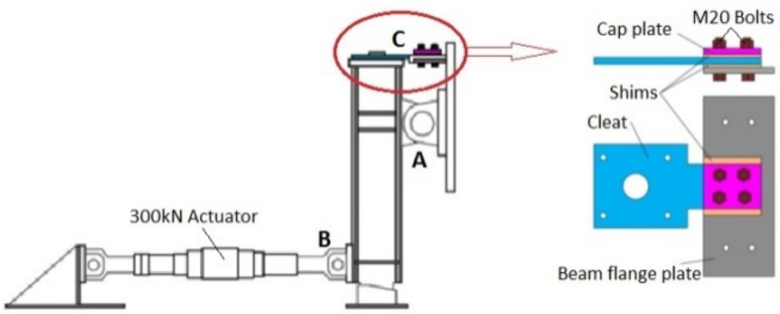

(a) (b)

Figure 4. SHJ's AFC test setup (a), schematic of the SHJ's AFC test specimens (b)

Table 1. Nominal characteristics of the galvanized HSFG PC 8.8 structural steel bolts

Bolt Size	Shank Area	Stress Area of Thread	Pitch	Tensile Strength (minimum)	Yield Stress (minimum)	Proof Load Stress	Average Ultimate Tensile Stress (min×1.12)	Proof Load
	mm^2	*mm^2*	*mm*	*MPa*	*MPa*	*MPa*	*MPa*	*kN*
M20	314	245	2.5	830	660	600	930	147

Table 2. Characteristics of each BeS "M20-52-6.0NF/S1"

Part Number	Material	Rockwell Hardness	Finish	Inside Diameter (*mm*)	Outside Diameter (*mm*)	Overall Height (*mm*)	Thickness (*mm*)	Maximum Deflection (*mm*)	Load (100%) (*kN*)
M20-52-6.0NF/S1	AISI 4140	Rc 44-48	Mechanically Zinc Plated with clear chromate (ASTM B695, Class 12)	20.75	52.705	6.828	5.99	0.838	124.7

Table 3. Load-deflection values of the BeS "M20-52-6.0NF/S1"

Loading	**Load**(*kN*)	0	30.2	55.7	85.4	107	125
	Deflection(*mm*)	0	0.23	0.43	0.63	0.76	0.84
Unloading	**Load**(*kN*)	111	89	66.7	40	26.7	0
	Deflection(*mm*)	0.79	0.68	0.56	0.38	0.25	0

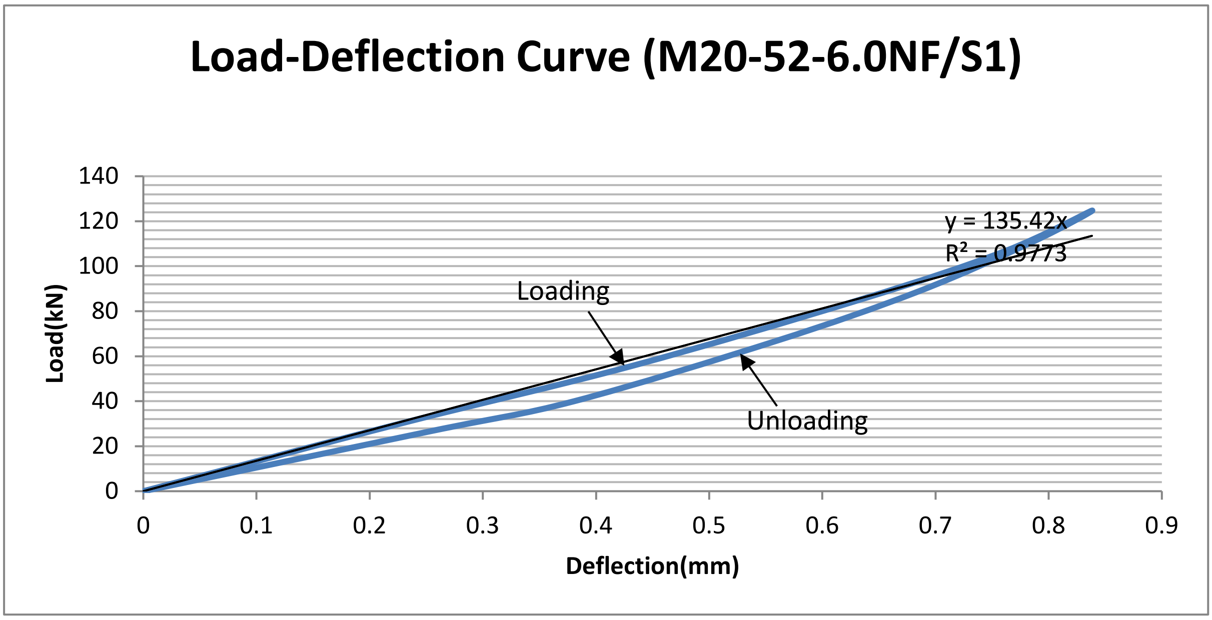

Figure 5. Loading and unloading curves of the BeS along with the fitted stiffness line

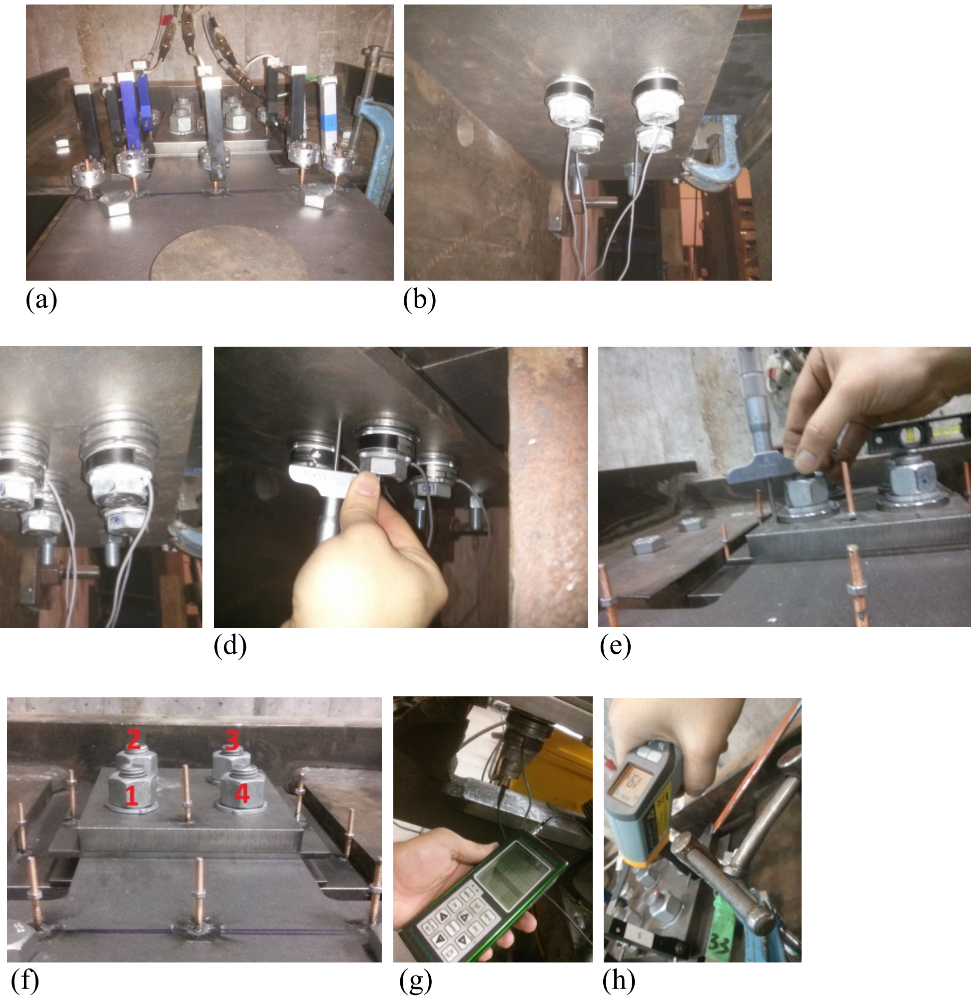

Figure 6. SHJ's AFC assembled component with portal gauges installed (NS or S1 or S3 configurations) (a), SHJ's AFC bolts at head side with donut load cells (NS configuration) (b), and (S3 or S4 configurations) (c), using depth micrometer to measure BeSs deflections at SHJ's AFC bolts' head side (S1 or S2 configurations) (d), using depth micrometer to measure BeSs deflections at SHJ's AFC bolts' nut side (S2 or S4 configurations) (e), SHJ's AFC bolts numbering (NS or S1 or S3 configurations) (f), using G5 ultrasound bolt tension meter to measure SHJ's AFC bolts lengths (g), and using digital infrared laser guided temperature gun to measure bolts temperature (h).

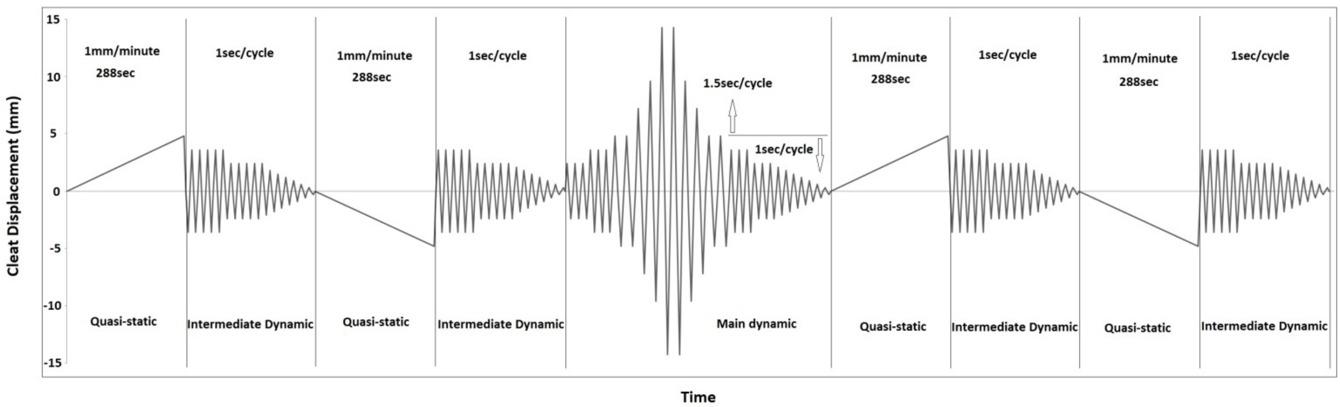

Figure 7. The loading regime consisting of quasi-static, intermediate dynamic, and main dynamic displacement controlled load histories

Table 4. Details of the test specimens

Specimen name	A AFC installed clamping force	B Average AFC installed bolt tension		C Nominal stiffness of the BeS system	D Average nominal BeS system deflection at installation	E Average nominal reserved deflection of the BeS system at installation
	kN	kN	% of bolt proof load	kN/mm	mm	mm
NS-T1	282	70.5	48	NA	NA	NA
NS-T2	296	74	50	NA	NA	NA
NS-T3	299	74.75	51	NA	NA	NA
S1-T1	278	69.5	47	135	0.52	0.32
S2-T1	292	73	50	67.5	1.09	0.58
S3-T1	288	72	49	45	1.62	0.90
S4-T1	285	71.25	48	33.8	2.14	1.21
S4-T2	306	76.5	52	33.8	2.28	1.07
S4-T3	316	79	54	33.8	2.35	1.01

Table 5. Percentage of post-sliding AFC clamping force loss, normalized force threshold of losing stiffness, and elastic strength reduction factor.

Specimen name	Percentage of clamping force loss (CFL)				Normalized elastic strength limit (ESL)				Elastic strength reduction factor (SRF)			
	Value	Mean	Standard deviation	Coefficient of variation	Value	Mean	Standard deviation	Coefficient of variation	Value	Mean	Standard deviation	Coefficient of variation
NS-T1	59.9				0.40				148.2			
NS-T2	55.1	58.6	2.5	0.04	0.27	0.37	0.07	0.19	203.8	165.1	27.4	0.17
NS-T3	60.9				0.42				143.3			
S1-T1	69.8	-	-	-	0.51	-	-	-	136.6	-	-	-
S2-T1	63.8	-	-	-	0.41	-	-	-	155.5	-	-	-
S3-T1	36.1	-	-	-	0.51	-	-	-	70.7	-	-	-
S4-T1	41.4				0.52				79.2			
S4-T2	31.4	37.5	4.4	0.12	0.63	0.59	0.05	0.08	49.5	64.5	12.1	0.19
S4-T3	39.9				0.61				64.9			

Note: The values shown in red might have been influenced by the low accuracy of the donut load cells at low level of bolt tension

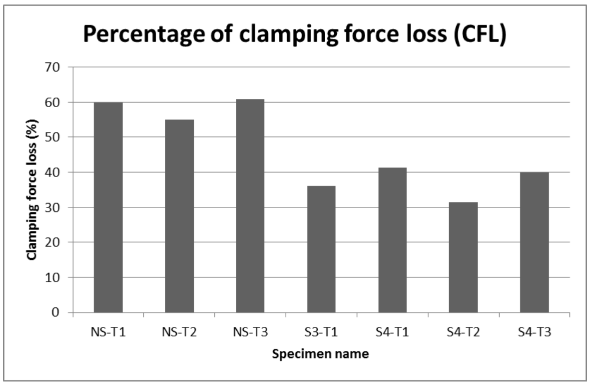

(a)

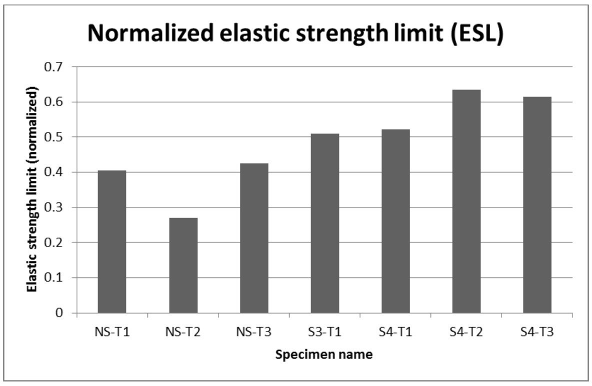

(b)

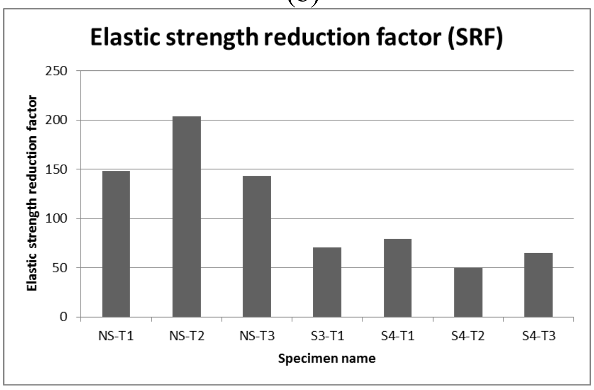

(c)

Figure 8. SHJ's AFC normalized clamping force loss (a) and elastic strength limit (b), and elastic strength reduction factor (c)

Table 6. Percentage of SHJ’s AFC stable sliding maximum total bolt tension increase and average stable sliding normalized force..

Specimen name	percentage of AFC stable sliding (SS) maximum total bolt tension increase				Average AFC stable sliding (SS) normalized force					
	Value	*Mean*	*Standard deviation*	*Coefficient of variation*	*Value (+ve)*	*Value (-ve)*	*Value (Average)*	*Mean*	*Standard deviation*	*Coefficient of variation*
NS-T1	53.4				1.0	0.9	1.0			
NS-T2	60.1	53.0	6.0	0.11	1.1	0.9	1.0	1.04	0.05	0.05
NS-T3	45.4				1.2	1.0	1.1			
S1-T1	22.6	-	-	-	1.3	1.1	1.2	-	-	-
S2-T1	30.1	-	-	-	1.1	1.0	1.1	-	-	-
S3-T1	16.2	-	-	-	1.1	0.8	1.0	-	-	-
S4-T1	14.8				1.2	1.0	1.1			
S4-T2	6.1	13.7	5.8	0.42	1.1	1.0	1.1	1.14	0.09	0.08
S4-T3	20.1				1.3	1.2	1.3			

Note: The values shown in red might have been influenced by the low accuracy of the donut load cells at low level of bolt tension

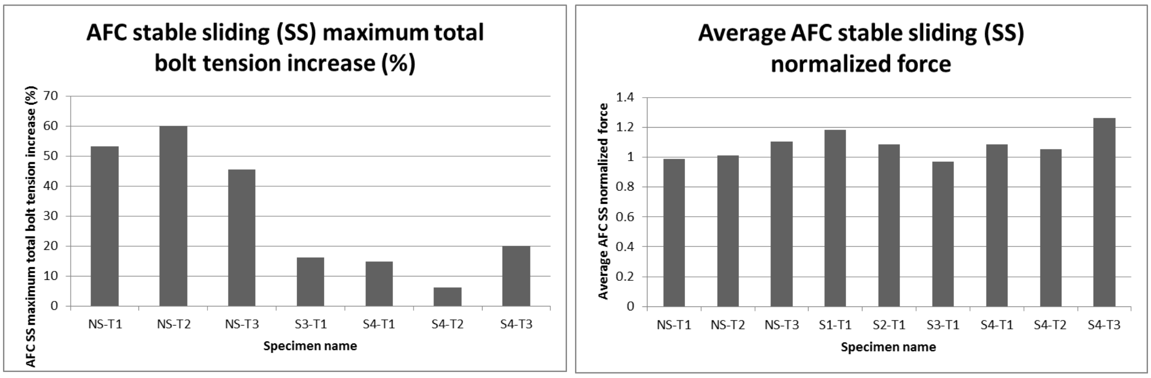

(a) (b)

Figure 9. SHJ’s AFC stable sliding maximum total bolt tension increase (a) and average stable sliding normalized force (b)

Table 7. SHJ’s AFC average stable sliding coefficient of friction.

Specimen name	Average stable sliding (SS) system coefficient of friction (CoF)					
	Value (+ve)	*Value (-ve)*	*Value (Average)*	*Mean*	*Standard deviation*	*Coefficient of variation*
NS-T1	0.60	-0.56	0.58			
NS-T2	0.67	-0.37	0.52	0.58	0.05	0.08
NS-T3	0.80	-0.48	0.64			
S1-T1	1.59	-0.82	1.21	-	-	-
S2-T1	1.30	-1.11	1.21	-	-	-
S3-T1	0.65	-0.54	0.59	-	-	-
S4-T1	0.80	-0.63	0.71			
S4-T2	0.80	-0.60	0.70	0.72	0.02	0.03
S4-T3	0.93	-0.58	0.75			

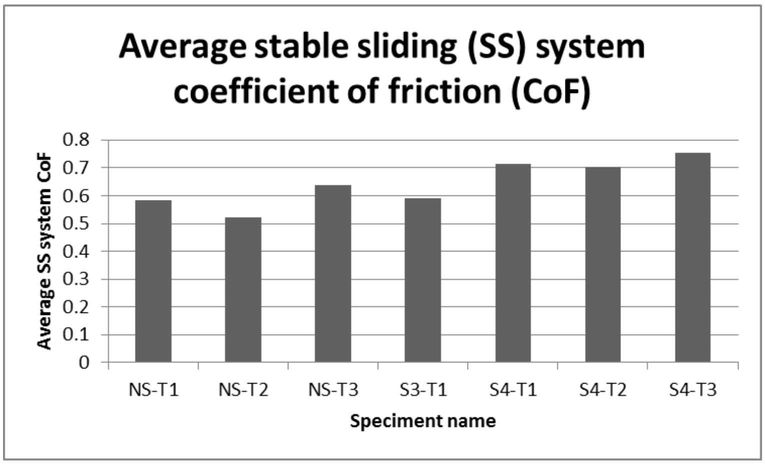

Figure 10. SHJ's AFC average stable sliding coefficient of friction.

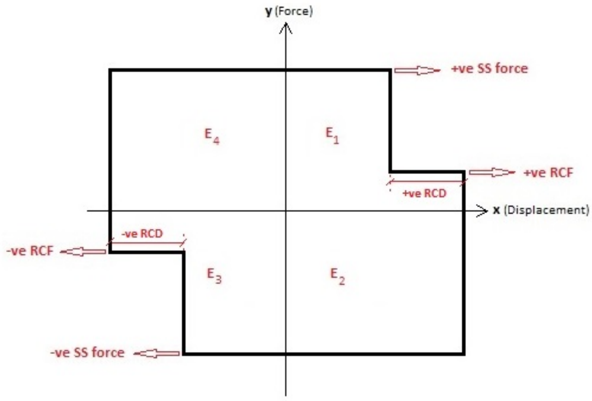

Figure 11. SHJ's AFC schematic stable slding hystheresis loop showing stable sliding force, re-centering force, recentring distance, and dissipated energy in each quadrant.

Table 8. SHJ's AFC re-centering energy ratio, normalized re-centering force, normalized recentering distance, and self-centering factor.

Specimen name	Re-Centering Energy Ratio (RCER)			Normalized Re-Centering Force (RCF)			Normalized Re-Centering Distance (RCD)			Self-Centering Factor (SCF)
	E1+E3	*E2+E4*	*RCER*	*RCF (+ve)*	*RCF (-ve)*	*RCF (average)*	*RCD (+ve)*	*RCD (-ve)*	*RCD (average)*	*SCF (average)*
	Joule (J)									
NS-T1	6378	7967	0.80	0.33	0.32	0.33	0.42	0.43	0.42	0.62
NS-T2	6821	8463	0.81	0.41	0.40	0.41	0.52	0.54	0.53	0.61
NS-T3	7374	9267	0.80	0.37	0.35	0.36	0.56	0.55	0.56	0.51
S1-T1	6822	9323	0.73	0.26	0.19	0.22	0.58	0.63	0.60	0.27
S2-T1	5373	8473	0.63	0.06	0.07	0.06	0.60	0.68	0.64	0.06
S3-T1	5803	7996	0.73	0.18	0.19	0.19	0.62	0.57	0.59	0.23
S4-T1	6146	8737	0.70	0.19	0.14	0.16	0.63	0.56	0.59	0.19
S4-T2	7112	9174	0.78	0.26	0.26	0.26	0.61	0.57	0.59	0.34
S4-T3	8236	11293	0.73	0.26	0.25	0.26	0.67	0.68	0.68	0.28

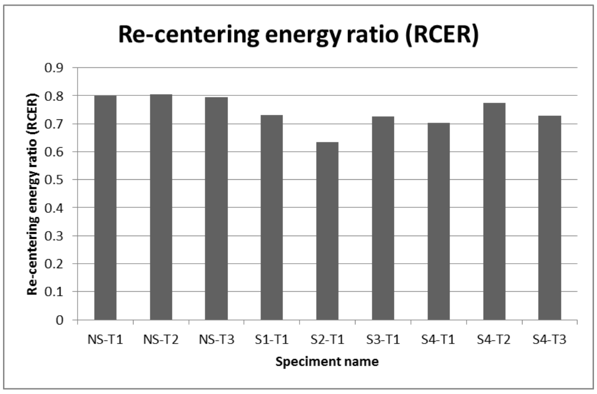

(a)

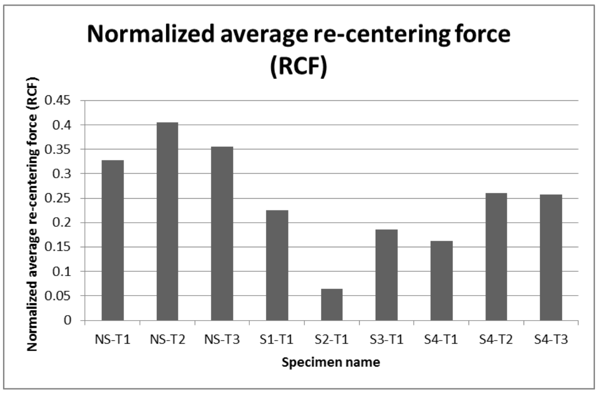

(b)

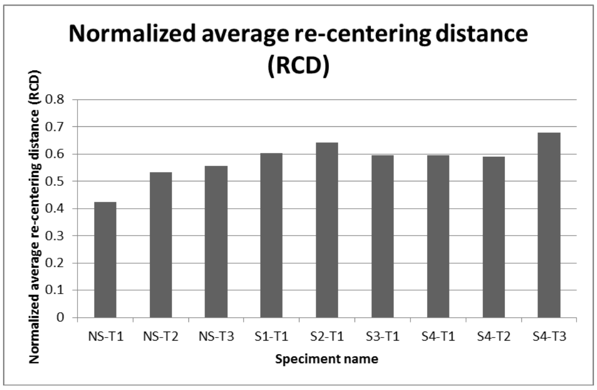

(c)

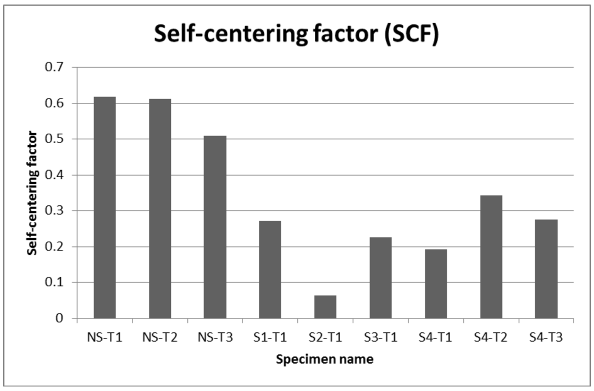

(d)

Figure 12. SHJ's AFC re-centering energy ratio (a), normalized average re-centering force (b), normalized average recentering distance (c), and self-centering factor (d).

Figure 13. extent of the slding resulted scratches on the abrasion resistant shim facing the cleat at the SHJ beam bottom flange side for the NS configuaration (left) and S2 configuration (right).

References

1. MacRae, G. and C. Clifton, *Low Damage Design of Steel Structures*. 2013, Steel Construction New Zealand: Steel Innovations 2013 Workshop, Christchurch, New Zealand.
2. Hamburger, R.O. and K. Frank. *Performance of Welded Steel Moment Connections - Issues Related to Materials and Mechanical Properties*. in *The Workshop on Steel Seismic Issues*. 1994. USA.

3. Engelhardt, M.D., *Ductile Detailing of Steel Moment Frames: Basic Concepts, Recent Developments and Unresolved Issues*, in *XIII Mexican Conference on Earthquake Engineering*. 2001: Guadalajara, Mexico.
4. Roeder, C., *Connection Performance for Seismic Design of Steel Moment Frames.* Journal of Structural Engineering, 2002. **128**(4): p. 517-525.
5. Yang, T.-S. and E.P. Popov, *Experimental and Analytical Studies of Steel Connections and Energy Dissipators*. 1995, Earthquake Engineering Research Center: Berkeley, University of California.
6. Clifton, G.C., *Semi-rigid joints for moment-resisting steel framed seismic-resisting systems*, in *Department of Civil and Environmental Engineering*. 2005, University of Auckland: Auckland, New Zealand.
7. Pall, A.S., *Limited Slip Bolted Joints - A Device to Control the Seismic Response of Large Panel Structures*, in *Centre for Building Studies*. 1979, Concordia University: Montreal, Quebec, Canada.
8. Pall, A.S. and C. Marsh, *Response of friction damped braced frames.* Journal of Structural Engineering, 1982. **108**(9): p. 1313-1323.
9. Filiatrault, A. and S. Cherry, *Performance Evaluation of Friction Damped Braced Steel Frames Under Simulated Earthquake Loads.* Earthquake Spectra, 1987. **3**(1): p. 57-78.
10. FitzGerald, T.F., T. Anagnos, M. Goodson, and T. Zsutty, *Slotted Bolted Connections in Aseismic Design for Concentrically Braced Connections.* Earthquake Spectra, 1989. **5**(2): p. 383-391.
11. Christopoulos, C., R. Tremblay, H.-J. Kim, and M. Lacerte, *Self-centering energy dissipative bracing system for the seismic resistance of structures: development and validation.* Journal of Structural Engineering, 2008. **134**(1): p. 96-107.
12. MacRae, G.A., G.C. Clifton, H. Mackinven, N. Mago, J. Butterworth, and S. Pampanin, *The Sliding Hinge Joint Moment Connection.* Bulletin of the New Zealand Society for Earthquake Engineering, 2010. **43**(3): p. 202.
13. Latour, M., V. Piluso, and G. Rizzano, *Experimental analysis on friction materials for supplemental damping devices.* Construction and Building Materials, 2014. **65**: p. 159-176.
14. Grigorian, C.E. and E.P. Popov, *Energy dissipation with slotted bolted connections*. 1994, Earthquake Engineering Research Centre: Berkeley, California.
15. Khoo, H.H., C. Clifton, J. Butterworth, G. MacRae, and G. Ferguson, *Influence of steel shim hardness on the Sliding Hinge Joint performance.* Journal of Constructional Steel Research, 2012. **72**: p. 119-129.
16. Iyama, J., C.Y. Seo, J.M. Ricles, and R. Sause, *Self-centering MRFs with bottom flange friction devices under earthquake loading.* Journal of Constructional Steel Research, 2009. **65**(2): p. 314-325.
17. Tsai, K.C., C.C. Chou, C.L. Lin, P.C. Chen, and S.J. Jhang, *Seismic self‐centering steel beam‐to‐column moment connections using bolted friction devices.* Earthquake Engineering & Structural Dynamics, 2008. **37**(4): p. 627-645.
18. Rojas, P., J. Ricles, and R. Sause, *Seismic performance of post-tensioned steel moment resisting frames with friction devices.* Journal of Structural Engineering, 2005. **131**(4): p. 529-540.
19. Wolski, M., J.M. Ricles, and R. Sause, *Experimental study of a self-centering beam–column connection with bottom flange friction device.* Journal of Structural Engineering, 2009. **135**(5): p. 479-488.
20. Tremblay, R., M. Lacerte, and C. Christopoulos, *Seismic response of multistory buildings with self-centering energy dissipative steel braces.* Journal of Structural Engineering, 2008. **134**(1): p. 108-120.

21. Golondrino, J.C., G.A. MacRae, J.G. Chase, G.W. Rodgers, and G.C. Clifton, *Hysteretic Behavior of Symmetrical Friction Connections (SFC) Using Different Steel Grade Shims*, in *10th Pacific Structural Steel Conference*. 2013: Singapore.
22. Zhu, S. and Y. Zhang, *Seismic analysis of concentrically braced frame systems with self-centering friction damping braces.* Journal of Structural Engineering, 2008. **134**(1): p. 121-131.
23. Loo, W.Y., P. Quenneville, and N. Chouw, *A new type of symmetric slip-friction connector.* Journal of Constructional Steel Research, 2014. **94**: p. 11-22.
24. Leung, H.K., G.C. Clifton, H.H. Khoo, and G.A. MacRae, *Experimental Studies of Eccentrically Braced Frame with Rotational Bolted Active Links*, in *8th International Conference on Behavior of Steel Structures in Seismic Areas (STESSA)*. 2015: Shanghai, China.
25. Borzouie, J., G.A. MacRae, J. Chase, G. Rodgers, and G.C. Clifton, *Experimental Studies on Cyclic Performance of Column Base Strong Axis–Aligned Asymmetric Friction Connections.* Journal of Structural Engineering, 2015. **0**(0): p. 04015078.
26. Borzouie, J., G.A. MacRae, J.G. Chase, G.W. Rodgers, and G.C. Clifton, *Experimental studies on cyclic performance of column base weak axis aligned asymmetric friction connection.* Journal of Constructional Steel Research, 2015. **112**: p. 252-262.
27. Golondrino, J.C., R. Xie, G.A. MacRae, G. Chase, G. Rodgers, and C. Clifton, *Braced Frame Using Asymmetrical Friction Connections (AFC)*, in *8th Conference on Behaviour of Steel Structures in Seismic Areas (STESSA)*. 2015: Shanghai, China.
28. Khoo, H.H., *Development of the low damage self-centering Sliding Hinge Joint*, in *Department of Civil and Environmental Engineering*. 2013, University of Auckland: Auckland, New Zealand.
29. Khoo, H.H., C. Clifton, J. Butterworth, G. MacRae, S. Gledhill, and G. Sidwell, *Development of the self-centering Sliding Hinge Joint with friction ring springs.* Journal of Constructional Steel Research, 2012. **78**: p. 201-211.
30. Tremblay, R., *Seismic behavior and design of friction concentrically braced frames for steel buildings*. 1993, The University of British Columbia.
31. Ferrante Cavallaro, G., A. Francavilla, M. Latour, V. Piluso, and G. Rizzano, *Experimental behaviour of innovative thermal spray coating materials for FREEDAM joints.* Composites Part B: Engineering, 2017. **115**: p. 289-299.
32. Latour, M., V. Piluso, and G. Rizzano, *Free from damage beam-to-column joints: Testing and design of DST connections with friction pads.* Engineering Structures, 2015. **85**: p. 219-233.
33. Ramhormozian, S., G.C. Clifton, G.A. MacRae, and G.P. Davet, *Stiffness-based approach for Belleville springs use in friction sliding structural connections.* Journal of Constructional Steel Research, 2017. **138**(Supplement C): p. 340-356.
34. NZS3404. *Steel structures standard, incorporating Amendments 1 and 2*. 1997/2001/2007. Wellington [N.Z.]: Standards New Zealand.
35. Butterworth, J.W. and G.C. Clifton, *Performance of Hierarchical Friction Dissipating Joints in Moment Resisting Steel Frames*, in *12th World Conference on Earthquake Engineering (12WCEE)*. 2000: Auckland, New Zealand.
36. Chopra, A.K., *Dynamics of Structures: Theory and Applications to Earthquake Engineering*. 2007: Pearson/Prentice Hall.
37. NZS/AS-1627.9:1989, *Metal finishing - Preparation and pretreatment of surfaces - Pictorial surface preparation standards for painting steel surfaces*. 1989.
38. AS/NZS1252, *High-strength steel bolts with associated nuts and washers for structural engineering*, in *Australia/New Zealand Standard*. 1996.
39. NZS1170.5:2004, *Structural Design Actions - Part 5: Earthquake design actions*. 2004, Standards New Zealand: New Zealand.
40. SAC-Joint-Venture, *Recommended design criteria for new steel moment frame structures*. 2000: Washington, D.C.

41. Ramhormozian, S., G.C. Clifton, B. Bergen, M. White, and G.A. Macrae, *An Experimental Study on the Asymmetric Friction Connection (AFC) Optimum Installed Bolt Tension*, in *NZSEE Annual Technical Conference and 15th World Conference on Seismic Isolation, Energy Dissipation and Active Vibration Control of Structures*. 2017: Wellington, New Zealand.
42. Allain, R., *Friction Isn't Always What You Think It Is.* DOT PHYSICS, 2014.
43. Khoo, H.H., C. Clifton, G. MacRae, H. Zhou, and S. Ramhormozian, *Proposed design models for the asymmetric friction connection.* Earthquake Engineering & Structural Dynamics, 2014.